Ocean and Coastal Management 273 (2026) 108062

Contents lists available at ScienceDirect

Ocean and Coastal Management

journal homepage: www.elsevier.com/locate/ocecoaman

The fate of tidal flats under reduced sediment supply and human activities in the bifurcated Yangtze Estuary

Chunyan Zhu [a], Weiming Xie [a,*], Leicheng Guo [a], Dirk Sebastiaan van Maren [b,c], Wenting Wu [d], Fan Xu [a], Yuan Xu [a], Naiyu Zhang [a], Zheng Bing Wang [b,c], Qing He [a]

[a] State Key Laboratory of Estuarine and Coastal Research, East China Normal University, Shanghai, 200241, China
[b] Faculty of Civil Engineering and Geosciences, Delft University of Technology, Delft, 2600GA, the Netherlands
[c] Deltares, Delft, the Netherlands
[d] Key Laboratory of Spatial Data Mining and Information Sharing of Ministry of Education, National & Local Joint Engineering Research Center of Satellite Geospatial Information Technology, Fuzhou University, Fuzhou, China

ARTICLE INFO

Keywords:
Tidal flat
Sediment supply
Yangtze estuary
Human activities
Navigation channel

ABSTRACT

Tidal flats provide essential ecosystem services but are increasingly threatened by reduced sediment supply and human activities, requiring close monitoring and understandings in estuaries. We focus on the four tidal flats with a total area of 1800 km^2 in the Yangtze Estuary and systematically evaluate their morphodynamic evolution based on consistent bathymetry data over 60 years (1958–2022). While fluvial sediment supply has declined since the mid-1980s, all four tidal flats in the estuary sustained accretion until 2010, demonstrating a lag of 20–30 years in estuarine morphological response to sediment decline. However, note that accretion primarily occurs on higher parts of the shoals, whereas erosion dominates in the subtidal zones. This is mainly attributed to the combined impact of saltmarsh expansions, reclamation, and channel scour and dredging. It suggests that part of the eroded sediment from channels deposits on adjacent shoals, leading to a regional sediment budget balance, particularly in the central channel-shoal complex with the navigation channel. Moreover, the initiative of removing *Spartina* from the shoals, a fast-spreading invasive species that benefits shoal accretion but not native species, might disrupt the ongoing accretion of high shoals and induce overwhelming erosion and sediment loss. One management strategy to counteract these impacts and restore tidal flats is to make beneficial use of the dredged and trapped sediment from the North Passage, an annual amount of approximately 50 million m^3, to the adjacent shoals, though how to sustainably manage the sediments remains another concern.

1. Introduction

Tidal flats are valuable ecosystems that offer essential services for habitats and humans worldwide. These ecosystems are facing significant threats due to climate change and human interventions such as coastal development (Syvitski et al., 2022; Edmonds et al., 2023), reduced fluvial sediment fluxes (Besset et al., 2019; Dethier et al., 2022), and sea-level rise (Nienhuis et al., 2023). Approximately 16 % of global tidal flats were lost between 1984 and 2016 (Murray et al., 2019). However, tidal flat evolution exhibits strong spatial and temporal variations depending on their hydrodynamic forcing (de Vet et al., 2017; M. Zhang et al., 2021) and sediment supply (Gao, 2007; van Maren et al., 2013; Grandjean et al., 2024). Quantifying tidal flat evolution and in-depth understanding of the driving mechanisms are critical for addressing the effects of global change and restoring wetland ecosystems, thereby promoting sustainable coastal management.

The Yangtze Estuary is the mouth of the Yangtze River meeting the East China Sea, hosting megacities like Shanghai. It is characterized by large tidal flat systems in the mouth zone, the largest being eastern Chongming flat (CM), Hengsha shoal (HS), Jiuduan shoal (JD), and Nanhui flat (NH), with a total area of approximately 1800 km^2 (Fig. 1b). Herein 'shoals' are submerged or partially submerged long and narrow ridges that have not (yet) developed into full grown islands; 'tidal flats' are low-lying coastal areas exposed at low tide and flooded at high tide attached to the main land or a large island. In this study, CM and NH are therefore referred to as tidal flats and HS and JD are called shoals. These

This article is part of a special issue entitled: OD- MegaDelta Programme OCMA published in Ocean and Coastal Management.

* Corresponding author.
E-mail address: wmxie@sklec.ecnu.edu.cn (W. Xie).

https://doi.org/10.1016/j.ocecoaman.2025.108062
Received 15 September 2025; Received in revised form 23 November 2025; Accepted 17 December 2025
Available online 26 December 2025

shoals (and the estuary as a whole) used to develop over the past hundreds to thousand years in response to large river discharge events and fluvial sediment supply (~0.5 Gt yr^{-1}) (Chen et al., 1985; Guo et al., 2021). Dramatic changes occurred in the past decades predominantly due to increasing human activities. The fluvial sediment supply has decreased by 75 % since the mid-1980s, to 124 Mt yr^{-1} during 2003 and 2024 (Fig. 1a), due to >50,000 dams, particularly the Three Gorges Dam operation since 2003 (Yang et al., 2011).

The response of these shoals to reduced fluvial sediment supply in the Yangtze Estuary has been studied on a range of spatial scales as part of previous work. Wu et al. (2024a) used remote sensing to monitor the long-term areal developments of tidal flats, while Wang et al. (2021) explained the increase in tidal flat areas by an increase in saltmarsh area due to reduced human activities and increased conservation and restoration efforts. The evolution of shoals in the Yangtze Estuary has been extensively addressed on a local level based on bathymetric data, e.g., NH (Wei et al., 2017), JD (Li et al., 2016), HS (Yang et al., 2022), and CM (Xie et al., 2018) but also on an aggregated level accounting for the entire channel-shoal complex (Wei et al., 2015; Zhu et al., 2019). For instance, the NH's morphological changes were characterized by three stages of accretion with tidal channels developed during 2008–2013, which is attributed to fluctuating river discharge and cyclically altered hydrodynamics of the South Passage (SP) (Wei et al., 2017). The JD maintained a rapid or even accelerated area growth rate under reduced sediment supply due to sediment coarsening, sediment replenishment, saltmarsh growth etc. (X. Zhang et al., 2021). The HS shifted from horizontal expansion to vertical accretion during 1958–2019, dominated by adjacent large engineering works (Yang et al., 2022). The CM showed a decreased bed level change after embankment construction during 2012–2016; however, the sediment concentration was increasing, promoting CM accretion (Xie et al., 2018). These studies have indicated that although they are all largely accretionary, the individual shoals all develop differently, likely resulting from different hydrodynamics and local human interventions.

However, morphodynamic systems are coupled on various spatial scales, and understanding the response of morphological systems to human interventions requires an analysis on the appropriate spatial scale (Wang et al., 2015). For the Yangtze, this implies that the dynamics of a channel is coupled to its adjacent shoals, meaning that volumetric changes should not be evaluated over only an individual shoal or channel or aggregated to the channels and shoals in the whole mouth area, but over coupled channels-shoals (see also Mariotti and Fagherazzi, 2012; Lenstra et al., 2019; Zhou et al., 2021; Zhu et al., 2025). For instance, erosion and deposition vary strongly over depth (Zhu et al., 2019) in response to channel deepening, particularly the deepening of the North Passage (NP) in-between HS and JD due to the Deep Channel Navigation Project (DCNP). The DCNP implemented during 1997–2010 includes channel deepening from 6-7 m–12.5 m, two ~50 km long jetties, 19 groins, and a sediment barrier near the lower southern jetty (see Fig. 1b). Such deepening works should be evaluated on the scale of the NP including its adjacent shoals, but analyses on this particular spatial scale do not yet exist in the Yangtze Estuary (concentrating on

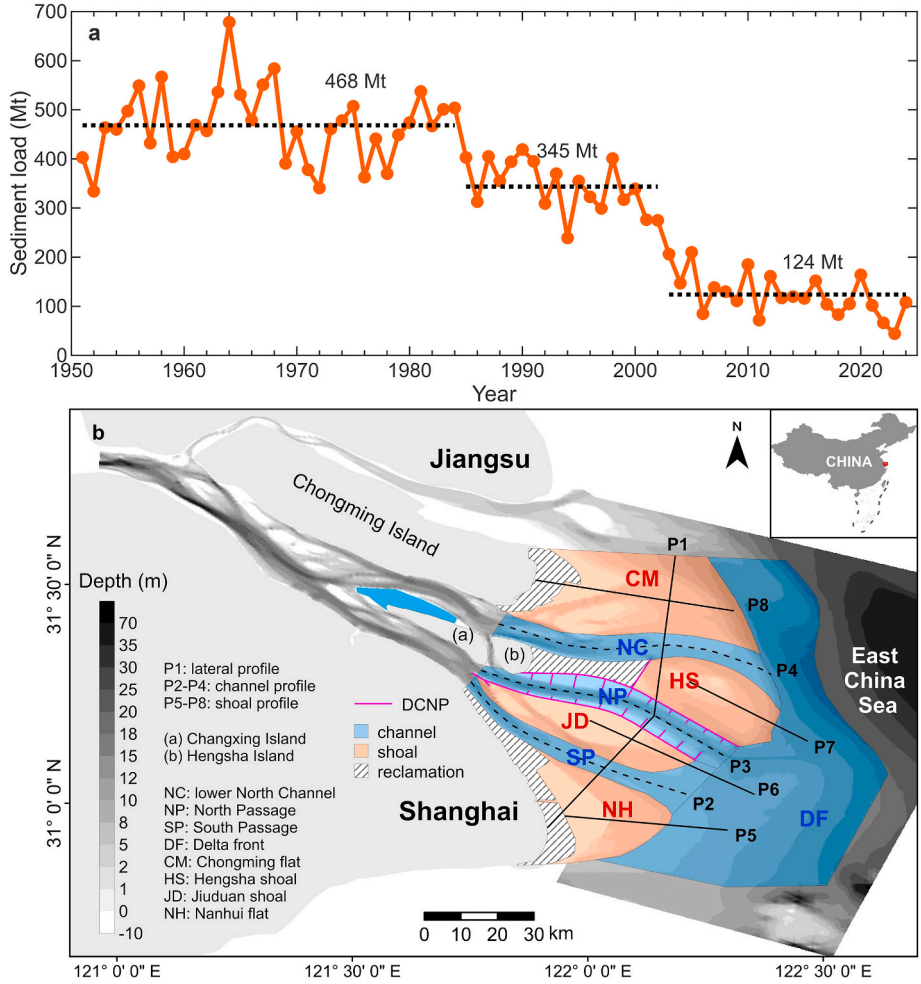

Fig. 1. **a** Sediment load at Datong station (~640 upstream of the estuary, tidal limit) during 1951–2024. The dotted reference lines indicate a stepwise decrease in sediment load during 1951–1984, 1984–2002, 2003–2024; **b** Study area in the Yangtze Estuary. P1~P8 transects are the lateral and longitudinal profiles for channels and shoals.

individual morphological units or the entire mouth area). Superimposed on these channel-shoal interactions is the large-scale morphological evolution of the estuary, tending to develop in the southward direction while maintaining its branching network (Chen et al., 1985; Zhu et al., 2025). This large-scale development is likely strongly influenced by the smaller-scale development of the channel-shoal complexes (in response to human interventions). Volumetric analyses covering these spatial scales and relationships have not yet been executed even though they are crucial for sustainable long-term estuarine management.

In this study, we therefore aim to systematically evaluate the evolution of four large-scale shoals in the mouth zone (i.e., CM, HS, JD, and NH) individually and jointly, and associate their evolution with ongoing channel development under reduced sediment supply and human activities in the bifurcated system. In combination with bathymetric data and remote sensing data, we quantify the sediment resources in the mouth zone to guide sustainable tidal flat management.

2. Data and methods

2.1. Bathymetry data

We collected bathymetry maps during 1958–2022, i.e., in 1958, 1978, 1986, 1997, 2002, 2010, 2013, 2016, 2019, and 2022. The bathymetric data from 1958 to 1997 were digitized from marine charts. The marine charts were digitized into depth points using the ArcGIS and Surfer software packages. The bathymetric data after 1997 were measured with echo sounders. The data were georeferenced using fixed landmarks that had related errors smaller than 0.01 cm, and then all the digitized data were transferred from their original projections into 'WGS 1984 UTM Zone 51N' using 'Projections and Transformations' in ArcGIS software. The depth points were interpolated to a digital elevation model (DEM) with a uniform 200 × 200 m grid resolution using kriging techniques. All bathymetric data derived from marine charts and sounding measurements were converted to theoretical lowest water level (TLWL). The difference between the TLWL and the mean water level decreases in the landward direction due to the landward decreasing tidal range. All depths used in this study (if not otherwise specified) are positive downward and relative to TLWL.

Based on the DEMs in different years, we can identify the changes in profiles and hypsometry. Hypsometry provides areal changes over a continuum of depth classes or isobaths. In the channel, the areal changes refer to the water surface, whereas on the shoals, the areal changes refer to the land surface. The difference between the hypsometry curves arises because of the erosion and deposition in the channels and shoals due to the geomorphic processes and/or human activities. Based on the DEMs of difference (DoD) method (Williams, 2012), which can be created by subtracting one elevation model from another, we can interpret the erosion and deposition pattern (difference of the water depth between DEMs in a period), channel or shoal volumes (sum of the water depth multiplied by the uniform grid cell areas), and net annual volumetric changes (sum of the difference of the water depth multiplied by the uniform grid cell areas divided by the number of years in a period).

The total errors of the bathymetric data come from stochastic errors due to individual data outliers, systematic errors introduced by the measuring instruments, and variable systematic errors consisting of user errors in measuring and handling the data (Colina Alonso et al., 2021; Elias et al., 2023). In this study, the marine charts from 1958 to 1997 record historical measurements with an accuracy of ±0.2 m. The echo sounders measuring bathymetry after 1997 have a vertical accuracy of ±0.1 m. The sounding positions, recorded by a theodolite for the 1958 and 1978 charts and a GPS (Trimble Navigation Limited, California, USA) for the remaining years, caused errors of 50 and < 1 m, respectively. The scales of the maps are 1:50,000 in 1978, 1986, and 1997 and 1:25,000 for the remaining maps, corresponding to a horizontal accuracy of 5 m and 2.5 m, respectively. The morphological units in this study are >50 km in horizontal dimension, and therefore a slight shift in the position of their boundaries, or shifts of the positions of the channels and shoals, is acceptable for the volume calculations. To enable reliable estimates of sedimentation-erosion trends and volume changes, we have also inspected the data in detail manually. Overall, the data accuracy is acceptable for calculation of accretion and erosion volumes on decadal time scales (especially given the relatively large volume changes).

2.2. Satellite-derived data

We obtain changes in bare flats and saltmarshes (including *Phragmites australis*, *Scirpus mariqueter*, *Spartina alterniflora*) from the dataset of land use changes during 1990–2020, which is the same dataset published earlier (Wu et al., 2024a). This dataset was generated using a phenology-based algorithm applied to Landsat time-series imagery and has a spatial resolution of 30 m and a temporal resolution of 2 years, and was robustly validated over the period 1990 to 2020. Specifically, they employed a rapid classification method, COLD-MC, to track land use change in the Yangtze Estuary. This method was implemented based on dense Landsat time-series imagery from 1990 to 2020. The approach integrates the Continuous Monitoring of Land Disturbance (COLD) algorithm to construct pixel-level time-series models and detect land cover changes with the Median Composite (MC) method to generate annual synthetic images that reduce noise from tidal turbidity. The temporal and spectral features were subsequently integrated and classified through the implementation of the Random Forest algorithm on the Google Earth Engine platform. This approach enabled the generation of high-accuracy land use change maps over the 30-year period.

Reclamation is quantified based on coastline changes using satellite images from 1990 to 2020 with an interval of 5 years. The coastline changes are detected using satellite images acquired during high tide with visual interpretation.

3. Results

3.1. Overall channel and shoal evolution

In the past 64 years, the channels have especially deepened and narrowed in the period of 2010–2022 compared to that of 1958–2002 (Fig. 2). Specifically, the width of the SP is reduced by 3.96 km on average after 2010, and the maximum reduction is 8.80 km in the middle segment of the channel (Fig. 2a). The averaged depth is 0.78 m deeper during 2010–2022 than that during 1958–2002, and the maximum depth increased by 2.09 m in the upper segment of the channel (Fig. 2d). The NP is strongly engineered, as the DCNP deepened and narrowed the navigation channel during 1997–2010. Consequently, the NP was narrowed by 4.76 km on average and up to 12.11 km (Fig. 2b), whereas it was deepened by 1.26 m on average and up to 4.4 m (Fig. 2e) in the longitudinal direction. The channel deepening and narrowing in the lower NC mainly occur near the landward limit of HS, with the maximum width reduction and depth increase of 7.88 km and 1.73 m, respectively (Fig. 2c and f). Overall, the SP, NP, and lower NC are narrowed by 47 %, 116 %, and 59 %, respectively, and deepened by 42 %, 125 %, and 43 %, respectively, in the period of 2010–2022 compared to that of 1958–2002. Therefore, among the three bifurcated channels, the strongest narrowing and deepening occur in the navigation channel.

The four large shoals in the mouth zone sustained accretion until 2010, although the fluvial sediment supply has decreased since the mid-1980s, suggesting a morphological response time lag of 20–30 years (Fig. 3). The CM, HS, and NH accreted until 2010 (CM, HS) or 2013 (NH), followed by erosion; present-day erosion rates are larger than historic sedimentation rates. At JD, the accretion rate rapidly decreased after 2010. Specifically, the growing rates of CM and HS are 16 million $m^3\ yr^{-1}$ and 8 million $m^3\ yr^{-1}$, respectively followed by an erosion rate of 19 million $m^3\ yr^{-1}$ and 11 million $m^3\ yr^{-1}$ during 2010–2022, respectively (Fig. 3a and b). The JD has been growing since 1958 with an accretion rate of 20 million $m^3\ yr^{-1}$ during 1958–2010 and a slower

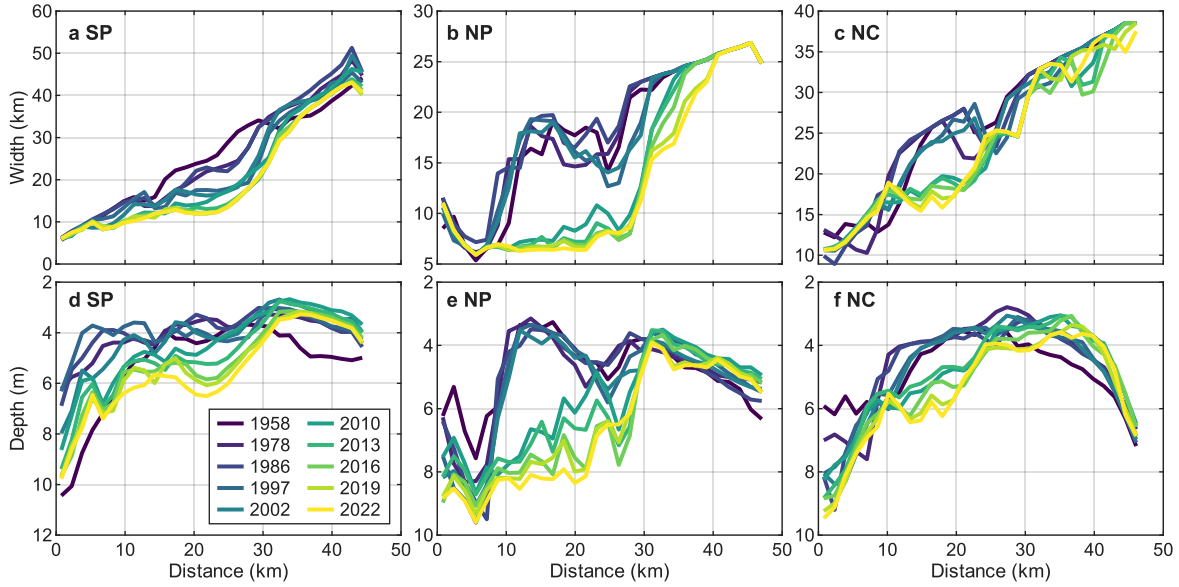

Fig. 2. Changes in cross-sectionally averaged channel **a, b, c** width and **d, e, f** depth below the theoretical lowest water level (TLWL) during 1958–2022 in the **a, d** South Passage (SP), **b, e** North Passage (NP), **e, f** lower North Channel (NC). See Fig. 1b for location of channels. X = 0 km is defined at the landward head of each channel.

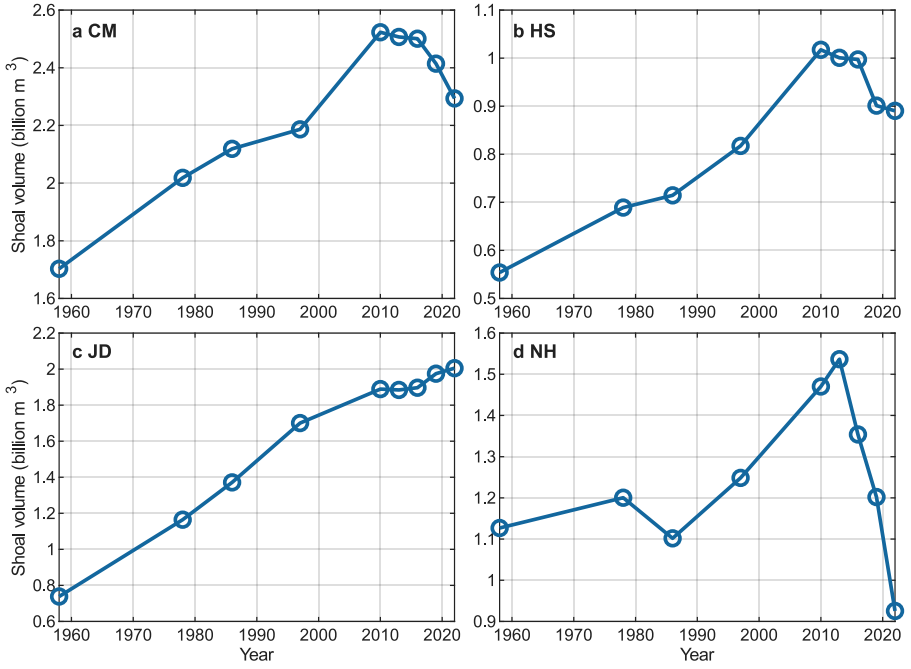

Fig. 3. Changes in shoal volumes above 6 m (below TLWL) during 1958–2022 in the **a** Chongming flat (CM), **b** Hengsha shoal (HS), **c** Jiuduan shoal (JD), **d** Nanhui flat (NH). The calculated regions of the shoals are indicated in Fig. 1b.

accretion rate of 10 million m^3 yr^{-1} during 2010–2022 (Fig. 3c). The NH accreted at a rate of 16 million m^3 yr^{-1} during 1986–2013, followed by a severe erosion rate of 68 million m^3 yr^{-1} during 2013–2022 (Fig. 3d). Therefore, the JD is the only shoal that still maintains accretion in sand volume while the other three are eroded. Overall, the four large-scale shoals have gained sediment of 2777 million m^3 during 1958–2010, with an accretion rate of 53.4 million m^3 yr^{-1}, and lost sediment of 1778 million m^3 during 2010–2022, with an erosion rate of 148.2 million m^3 yr^{-1}. It suggests that the four shoals are losing sediment at a much larger rate than they were accreted and built up.

Compared to the entire shoal evolution, the supratidal and intertidal flats are strongly influenced by reclamation and saltmarsh changes (Fig. 4). In the CM, reclamation mainly occurred during 1991–1992, 1998–2000, and 2012–2014 with increased reclaimed areas of 43 km^2, 24 km^2, 15 km^2, respectively (Fig. 4a). The saltmarsh area decreased from 66 km^2 to 24 km^2 by 64 % from 1991 to 2020, and the dominant species changed from *S. mariqueter* to *P. australis*. The bare flat areas show a decreasing trend before 2010 and an increasing trend afterwards, followed by a slight decrease in recent years. Although HS is mainly under water, its landward part was reclaimed with an area of 105.3 km^2 during 2003–2020 (Fig. 4b). Saltmarshes are only limitedly occupied on HS, with the largest area of 17 km^2 in 2020. The bare flat area decreased

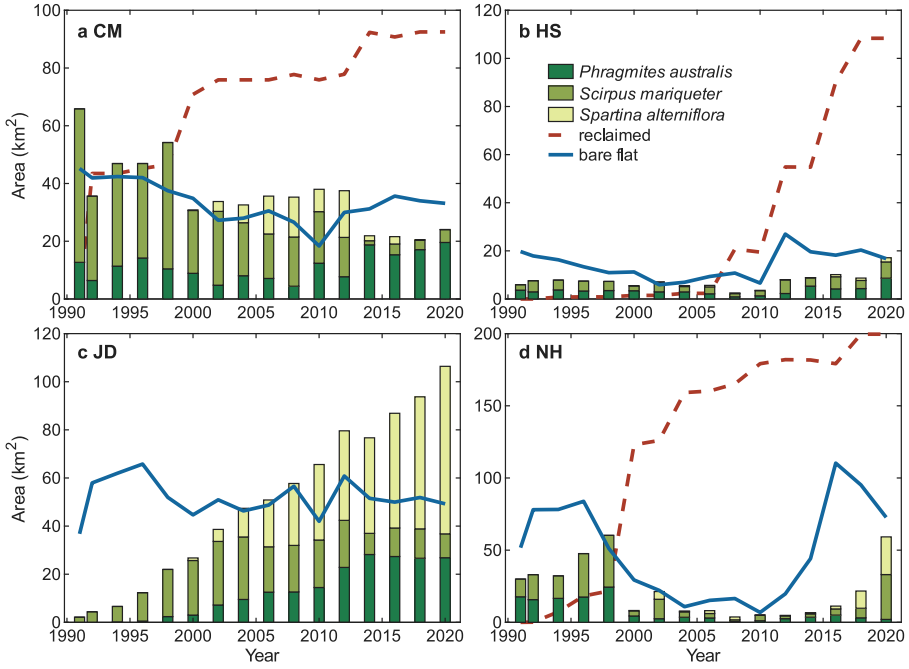

Fig. 4. Changes in reclaimed areas, vegetated areas (including *P. australis*, *S. mariqueter*, and *S. alterniflora*), and bare flat areas during 1991–2020 in the **a** Chongming flat (CM, region IV), **b** landward Hengsha shoal (HS, region III), **c** Jiuduan shoal (JD, region II), and **d** Nanhui flat (NH, region I). The regions I-IV are referred to Fig. 7.

except for an increase during 2010–2012. In the JD, saltmarsh kept developing with a stable increasing rate of nearly 4 km^2 yr^{-1} from 1996 to 2020, and the dominant species changed from *S. mariqueter* to *S. alterniflora* (Fig. 4c). The bare flat areas remained relatively unchanged during 2000–2008 and decreased during 2012–2020. In the NH, reclamation was most pronounced with an increased area reaching ~200 km^2 (Fig. 4d). Both the areas of saltmarsh and bare flat was strongly decreased from the late 1990s to 2010 and then strongly increased during 2010–2016. During 2016–2020, the saltmarsh area was increased by 48 km^2 whereas the bare flat area was decreased by 38 km^2. Overall, three of four shoals, i.e., CM, landward HS, and NH, are affected by reclamation, with land created by 93 km^2, 108 km^2, and 200 km^2, respectively since 1991. Saltmarshes develop on the CM, landward HS, JD, and NH, but the expansion of saltmarshes differs, and the dominant species changed particularly on CM and JD. The bare flat areas of four shoals have decreased in recent years and the decreasing trend even lasts for a longer period on CM and HS.

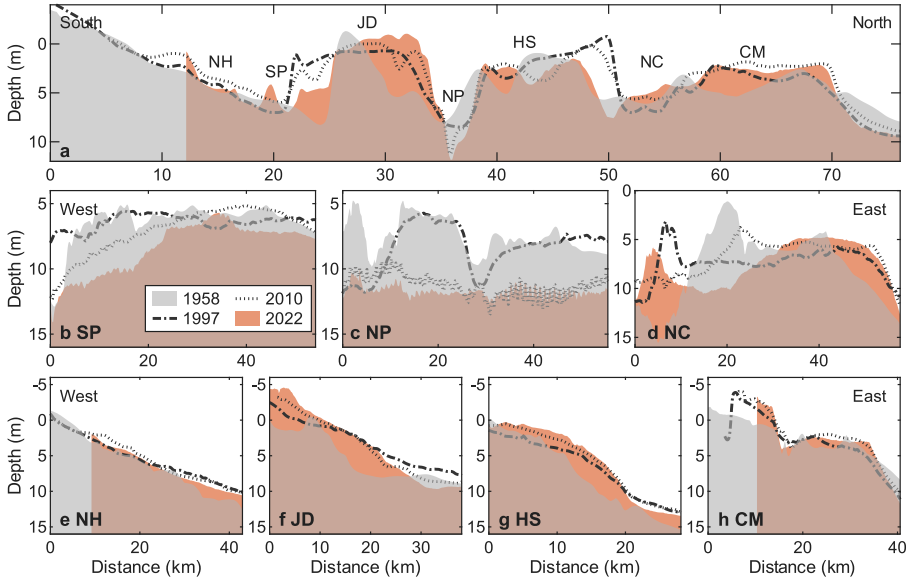

Fig. 5. Changes in profiles in representative years between 1958 and 2022: **a** lateral profile (P1) from the south to north; longitudinal profiles in the **b** South Passage (SP, P2), **c** North Passage (NP, P3), **d** lower North Channel (NC, P4), **e** Nanhui flat (NH, P5), **f** Jiuduan shoal (JD, P6), **g** Hengsha shoal (HS, P7), **h** Chongming flat (CM, P8). The profiles P1 (starting from the south), and P2-P8 (starting from the land side) are referred to Fig. 1b. Grey colors reflect areas with erosion between 1958 and 2022; brown colors sedimentation between 1958 and 2022. (For interpretation of the references to color in this figure legend, the reader is referred to the Web version of this article.)

3.2. Changes in longitudinal and lateral profiles

We interpret changes in longitudinal profiles along the thalweg in channels, cross-shore profiles perpendicular to isobaths on shoals, and lateral profiles mostly keeping perpendicular to the longitudinal profiles and covering all the channels and shoals (Fig. 5). The P1 transect shows the alternate channel-shoal structure in the longitudinal direction (Fig. 5a). The first 12 km from the south reflects the reclaimed processes in the NH, resulting in a milder lateral slope (~1/2000) compared to the other shoals. The SP is asymmetrically developed with significant bathymetric changes in the north side. The JD underwent pronounced deposition on both the north and south sides before 1997. Deposition has been enhanced on the northern JD since 1997, whereas erosion takes place in its south. The NP is developing towards a 'V'-shaped channel with deepening and narrowing. Severe erosion is observed in the northern NP or southern HS, and the slope remains steep (~1/300) after 1958. In contrast to the symmetric-to-asymmetric development in the JD, the HS is shifted from asymmetric to symmetric development as the historical northward elevation is strongly eroding. This erosion in the northern HS corresponds to the widening of the lower NC. The offshore of the eastern CM shows the lowest elevation, although accretion is enhanced until 2016. It is worthy to note that the slope of the northern CM becomes much steeper after 2010.

The bed profiles of the three main channels (P2-P4) illustrate the mouth bar evolution (Fig. 5b–d). In 1958, the minimum channel depths were approximately 5 m in the SP and NP and 4 m in the lower NC. The shallow parts occupied 40 km, 10 km, and 5 km in the SP, NP, and lower NC, respectively. During 1958–1997, the SP and NP experienced erosion whereas the NC accreted in the upstream and downstream sides of its mouth bar and the mouth bar was eroded. During 1997–2010, when the DCNP was implemented, the NP was deepened to 12.5 m (Fig. 5c). At the same time, the SP and lower NC eroded in their upstream reaches and accreted in the downstream reaches. During 2010–2022, the SP suffered continuous erosion, and the mouth bar became smaller, whereas the lower NC experienced erosion in its middle part. Overall, in the past 64 years, the mouth bar was removed in the NP because of erosion and dredging. Both the mouth bars in the SP and lower NC migrated seaward.

The shoal profiles (P5-P8) vary in shape and slope (Fig. 5e–h). The landward parts of the NH and CM were reclaimed successively in the recent decades. The NH is linearly shaped and developed under water (Fig. 5e). Since 1958, the slope of the NH has become steeper, from 1/4400 during 1958–1997 to 1/3000 in 2010. After 2016, the erosion at higher elevations leads to a milder slope in 2022. The JD shows a more convex-up shape before 2010 and becomes more linearly sloped after 2010 because of the siltation at middle to high elevations (Fig. 5f). The HS profile is relatively concave-up before 1997 and becomes more convex-up with more deposition at higher elevations after 2010 (Fig. 5g). Moreover, the HS is developed with a seaward advance, particularly during 1958–2010. During 2010–2022, the deposition mainly occurred at depths of 1–4 m of the HS, and the bed profile slope became steeper. Similar to the HS, the CM profile changed from a concave-up shape during 1958–1997 to a convex-up shape during 2010–2022 (Fig. 5h). The CM also developed a tidal channel, and the progradation is accompanied by a steeper slope at the edge.

3.3. Changes in hypsometry curves

The hypsometry curves provide areal changes over different depths, whereas the surface change is defined as the percentage of the surface area changes relative to its maximum during a period, implying the strength of vertical erosion and deposition (Fig. 6). For channels, the larger the surface area (water surface), the stronger the erosion. In the lower NC, the channel surface area was increasing at depths shallower than 5 m from 1958 to 2010, and the slope of the hypsometry curve is strongly increased, i.e., from a slope of 1/16 m/km^2 to nearly vertical

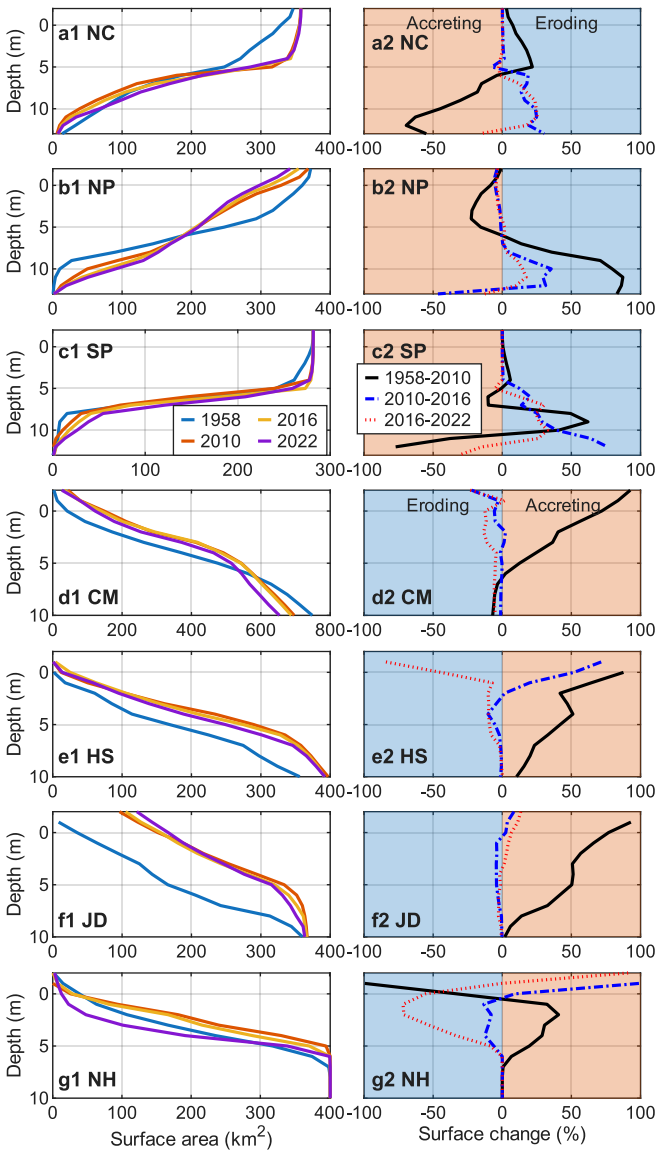

Fig. 6. Hypsometry curve (left panels) and the vertical surface changes (right panels) interpreted from the hypsometry curve in **a1, a2** lower North Channel (NC), **b1, b2** North Passage (NP), **c1, c2** South Passage (SP), **d1, d2** Chongming flat (CM), **e1, e2** Hengsha shoal (HS), **f1, f2** Jiuduan shoal (JD), **g1, g2** Nanhui flat (NH). The color shading for surface changes indicates eroding in blue and accreting in red. (For interpretation of the references to color in this figure legend, the reader is referred to the Web version of this article.)

lines (Fig. 6a). This indicates severe erosion in the shallow water in the lower NC, and the maximum erosion occurs at 5 m with the surface area reduced by 22 %. In deep water during 1958–2010, the lower NC was accreting with the surface area increased by a maximum of 70 % at 12 m. The erosion and accretion in the SP do not show a clear transition over depth, with a pronounced eroding effect between 7 m and 10 m and an accreting effect at depths deeper than 10 m. The largest increase in surface area is by 62 % at 9 m. After 2010, erosion dominates in deeper water in both the lower NC and SP, and the surface area is increased by a maximum of ~25 % at 10 m (2016–2022) and ~40 % at 10 m (2010–2016), respectively (Fig. 6a and c). In contrast, the NP is depositional at shallow water and erosional at deep water with the inflection depth of ~6 m since 1958 (Fig. 6b). The maximum deposition and erosion occurred during 1958–2010, with the surface area decreased by 22 % at 4 m and increased by 87 % at 11 m, respectively.

For shoals, the larger the surface area (land surface), the stronger the

accretion. From 1958 to 2010, the CM accreted at depths shallower than 6.5 m and eroded in deeper water (Fig. 6d), whereas the NH eroded at depths shallower than 0.5 m and accreted in deeper water (Fig. 6g). Note that the changes in surface area at 2 m above TLWL in NH reach 100 %, which is caused by the much smaller surface area with a magnitude of ~0.1 km^2. On the other hand, both HS and JD were accreting at all depths with an increase in surface area of 70 km^2 and 106 km^2 on average during 1958–2010, respectively (Fig. 6e and f). During 2010–2016, HS, JD, and NH accreted on higher shoals and eroded on lower shoals with the inflection depths of 2 m, 0 m, and 0.5 m, and the reduced surface areas were maximum of 10 % at 4 m, 4 % at 1–5 m, and 13 % at 1–4 m, respectively. After 2016, most shoals were eroding except for the shallower area of the JD (Fig. 6f). Most pronounced erosion occurred on higher HS and depths of 1–2 m of NH, corresponding to a reduction in surface area of 84 % and 71 %, respectively.

3.4. Changes in net erosion and deposition

The net erosion and deposition in the mouth zone is indicated in the periods of 1958–1997, 1997–2010, 2010–2016, and 2016–2022 (Fig. 7). During 1958–1997, only CM was reclaimed with an area of ~44 km^2 and the mouth zone was naturally developed with an overall sedimentation (Fig. 7a). The bed level change rate in the mouth zone ranges between −0.51 and 0.32 m yr^{-1} with an averaged value of 0.02 m yr^{-1}. The 10 m isobath migrated approximately 5 km seaward. In the period 1997–2010, the TGD started operation (in 2003) and the DCNP was implemented in the NP (from 1997 to 2010). Reclamation took place on CM, HS, and NH whereas *S. alterniflora* and *P. australis* were artificially introduced to JD in 1997 (Fig. 7b). In this period, accretion still dominated, but the maximum erosion and sedimentation rates were stronger (bed level change rate of −0.71~0.69 m yr^{-1}) than in the period of 1958–1997. Erosion mainly occurred in deep channels (particularly in the NP due to dredging) and seaward of the jetties. During 2010–2016, the bed level change rate was −2.02~1.53 m yr^{-1} with an averaged rate of −0.05 m yr^{-1} in the mouth zone. Erosion mainly occurred around the 10 m isobath (Fig. 7c). During 2016–2022, a sediment barrier was constructed in the southern jetty in the lower NP to block sediment exchange between NP and JD (Fig. 7d). The bed level change rate was −1.83~1.54 m yr^{-1} with an averaged rate of −0.03 m yr^{-1} in the mouth zone where erosion was stronger in the north than in the south.

The net erosion and deposition in the channels, delta front, and shoals as well as channel-shoal complexes are expressed as annual volumetric changes in Fig. 8. In the channels and on the delta front, except for the strongly engineered NP, alternative erosion and deposition took place before 1997 followed by an increasing erosion until 2013–2016. After this period, erosion rates decline and may even revert to deposition (e.g., NC, Fig. 8a). Moreover, net erosion in the delta front is an order of magnitude larger than that in the main channels (Fig. 8d). The NP experienced severe deposition until 2013, followed by a shift to slight erosion and severe accretion during 2016–2019 (Fig. 8b). The CM and NH shifted from accretion to erosion in 2013 which is later than the transition time occurred in the channels, reaching to a maximum net erosion of nearly 100 Mm^3 yr^{-1} during 2019–2022 (Fig. 8e and h). The HS shifted from accretion to erosion in 2010 (Fig. 8g), whereas the JD experienced a continuous accretion except for a slight erosion during 2010–2016 (Fig. 8f). The overall evolution of the HS and JD shows the

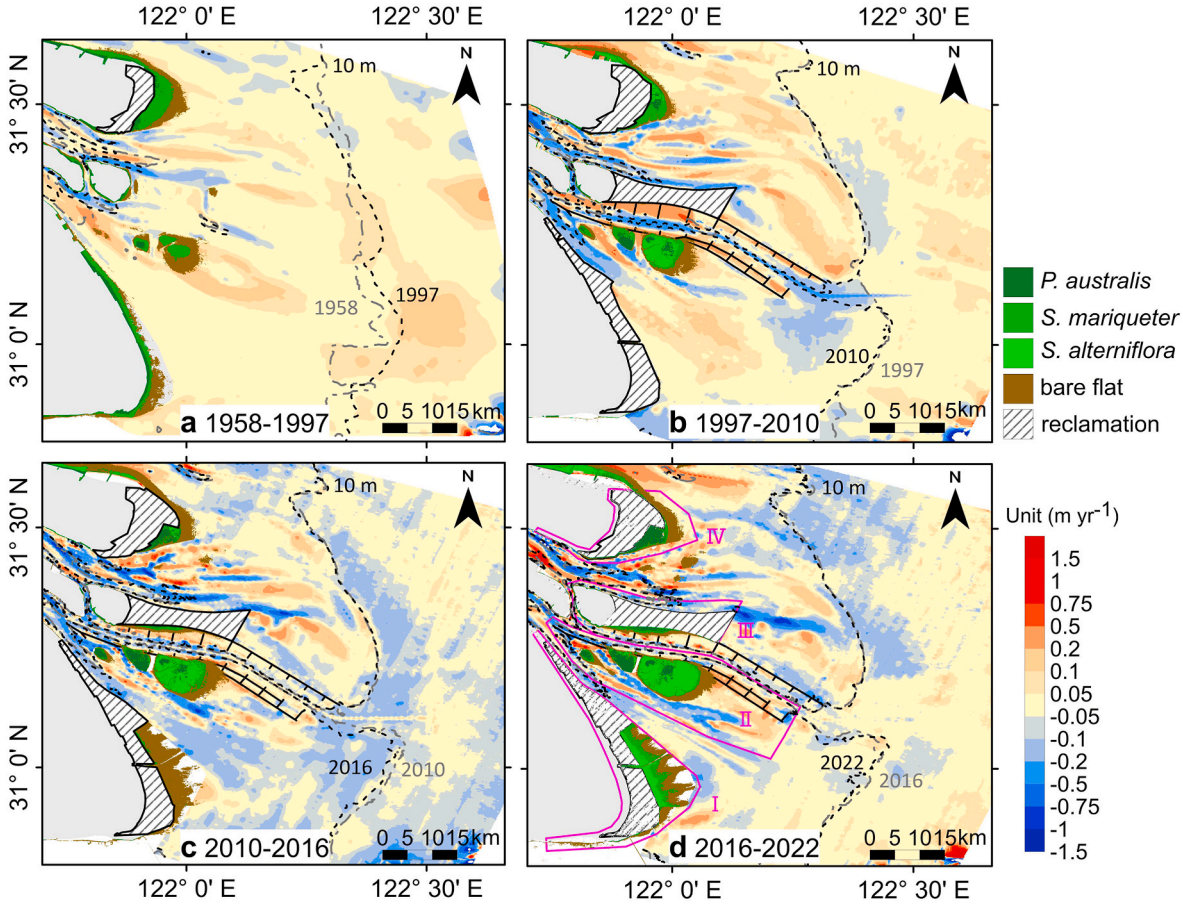

Fig. 7. The annual net erosion and deposition rate (m yr^{-1}) in the periods of **a** 1958–1997, **b** 1997–2010, **c** 2010–2016, **d** 2016–2022. The reclaimed areas (filled with diagonal lines), saltmarsh areas and bare flats are indicated in 1997, 2010, 2016, and 2022 for the four periods, respectively. The polygons in magenta are the regions to calculate the reclaimed, saltmarsh, and bare flat areas in the Nanhui flat (NH, I), Jiuduan shoal (JD, II), landward Hengsha shoal (HS, III) and Chongming flat (CM, IV), see Fig. 4.

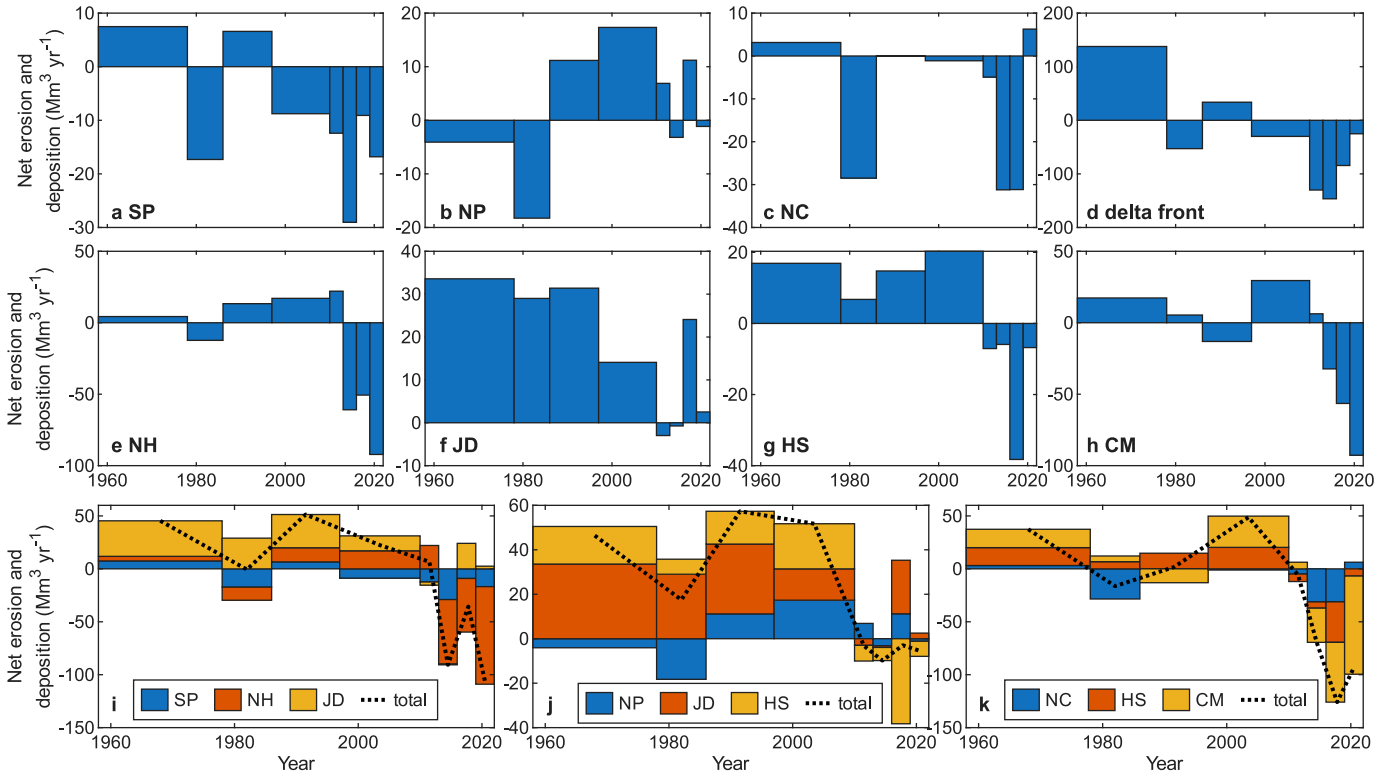

Fig. 8. Changes in net erosion and deposition ($Mm^3\ yr^{-1}$) in the **a** South Passage (SP), **b** North Passage (NP), **c** lower North Channel (NC), **d** delta front, **e** Nanhui flat (NH), **f** Jiuduan shoal (JD), **g** Hengsha shoal (HS), **h** Chongming flat (CM) and the channel-shoal complexes of **i** JD-SP-NH, **j** HS-NP-JD, **k** CM-NC-HS. The black dotted lines in **i**, **j**, **k** indicate the total net erosion and deposition among the channel-shoal complexes.

opposite trend: 1) the accretion before 2010 is enhanced in the HS but weakened in the JD and 2) the maximum erosion in the HS occurred during 2016–2019 when the maximum accretion occurred in the JD. Although these volumetric change per channel or shoal seems to reveal trends, they also show a large amount of variability. Therefore, these volumetric changes are subsequently evaluated over the channel-shoal complexes.

The volumetric changes of the northern complex (CM-NC-HS), central complex (HS-NP-JD) and southern complex (JD-SP-NH) show much clearer patterns (Fig. 8i–k). For all the complexes, the net accretion maintained relatively stable at ~50 $Mm^3\ yr^{-1}$ in 1958–2010 with the weakest accretion occurring during 1978–1986. After 2010, the northern and southern complexes keep losing sediment and the maximum net erosion reaches over 100 $Mm^3\ yr^{-1}$ in recent years (Fig. 8i and k). The erosion in the CM and NH dominates for the northern and southern complex, respectively. On the other hand, the sediment was nearly balanced in the central complex with a slight erosional rate of 6 $Mm^3\ yr^{-1}$ during 2010–2022 although strong erosion and accretion took place in the HS and JD, respectively during 2016–2019 (Fig. 8j).

4. Discussion

Our data reveal spatial patterns and temporal sediment volume changes in the mouth zone of the Yangtze Estuary. These patterns suggest spatial dependencies between the shoals and the channels which will be explored in detail in the following section. We will also relate temporal changes (notably the gradual decline in sedimentation rates) to local human interventions, a decline in (upstream) sediment supply, and to saltmarsh changes (especially the role of invasive species).

4.1. A sediment budget balance due to sediment exchanges

The shoal evolution is closely associated with channel evolution because of water and sediment exchange processes. All the channels in the mouth zone have been deepened and narrowed over the past 60 years (see Fig. 2). Many studies have discussed the positive feedback in sediment trapping and therefore high siltation due to deepening and narrowing in the Ems, Elbe, and Loire estuaries in Europe (Winterwerp and Wang, 2013; Winterwerp et al., 2013; de Jonge et al., 2014; van Maren et al., 2015). These studies reveal that channel deepening leads to tidal deformation with enhanced flood asymmetry favoring fine sediment import resulting in increasing sediment concentrations. The higher sediment concentration reduces the effective hydraulic drag, which in turn further strengthens tidal amplification and therefore increases suspended sediment concentrations. Similar effects of amplified tidal ranges due to channel deepening are also observed in the Hudson River estuary (Ralston et al., 2019), Gironde estuary (Jalón-Rojas et al., 2018) – see also Talke and Jay (2020) for their review on tidal changes. In the NP of the Yangtze Estuary, this positive feedback effect has also been identified with evidence of enhanced stratification, reduced hydraulic drag, and increased near-bed sediment concentrations after channel deepening and narrowing (Lin et al., 2021, 2025). Moreover, the high near-bed sediment concentration induces significant sediment-induced stratification which interacts with salinity-induced density stratification, further promoting high sediment concentration in the bottom layers of the water column (Zhu et al., 2021, 2022). Consequently, strong siltation occurred in the NP with high near-bed sediment concentrations of ~40 kg m^{-3}. Although deepening is most pronounced in the NP, the lower NC and SP are also deepened due to erosion (by approximately 40 %). But even after deepening the residual flow and sediment transport in the lower NC remains seaward, while the residual flow and sediment transport in the SP is only landward at neap tides (Zhou et al., 2025).

Note that the channels have been eroding since 1997, before the shoals started eroding. Except for the effect of dredging activities in the NP, this is also because the sediments trapped in the channels provide

sediment to the shoals due to sediment exchanges. Based on the satellite-derived surface sediment concentration published earlier (Luo et al., 2022), we find that the difference in surface sediment concentration between channels and shoals becomes smaller, even shifting to a regime with higher sediment concentration on shoals (Fig. 9). This new regime implies stronger sediment exchanges in the channel-shoal complexes under reduced sediment supply, likely caused by stronger tides and flood-directed flows which enhance channel-to-shoal sediment transport during flood and high water slack tide (Mariotti and Fagherazzi, 2012; Zhou et al., 2021).

Particularly in the central channel-shoal complex HS-NP-JD, the jetties in the NP have blocked the inter-channel exchanges and significantly altered the residual circulations (Zhu et al., 2018; Chen et al., 2020). Moreover, the elevated jetties play an important role in shifting from benefiting the northern shoal (HS) to promoting the southern shoal (JD) due to the clockwise residual horizontal circulation of sediment transport (Zhu et al., 2025). Therefore, the siltation in the navigation channel mainly benefits the long-term accretion of the JD rather than the other shoals. More importantly, the sediment exchanges between the navigation channel (NP) and the adjacent shoals lead to the sediment budget nearly balanced during 2010–2020.

4.2. Effect of land reclamation and saltmarshes

Land reclamation took place on CM, landward HS, and JD (see Figs. 4 and 7). The effect of reclamation on erosion in coastal environments is not straightforward, depending on the location of reclamation, hydrodynamic impacts, and sediment availability (van Maren et al., 2025). Specifically, land reclamation along estuarine channels usually often leads to tidal amplification, while reclamation in the upstream reaches decreases the tidal prism, promoting sedimentation; land reclamation in the places close to the estuary mouth and coasts reduces channel width, leading to an increase in flow velocities and probably triggering channel erosion. These different effects become complicated when tides are amplified as a large tidal range imports higher sediment while the increase in tidal flow velocity enhances bottom shear stress and reduces deposition (Fagherazzi and Priestas, 2010). Similar changes and feedback impact occurred in the Yangtze Estuary due to channel deepening (see section 4.1). However, regardless of the effect of land reclamation on erosion or sedimentation, it breaks the equilibrium profile of the shoals. For instance, the area above 0 m is growing rapidly, while the area shallower than 2 m is growing slowly, and the area shallower than 5 m is showing a decreasing trend (see Fig. 6). The slope of shoals becomes steeper (see Fig. 5), thereby less effectively dissipating wave energy, which is expected to increase due to more extreme weather under climate change. A similar phenomenon has also been found in other estuaries and coasts, e.g., the Fujian coast (Wu et al., 2024b), the Yellow River delta (Zhu et al., 2024).

Saltmarshes play an important role in sediment trapping and raising supratidal elevations (e.g., Zhu et al., 2019; Yang et al., 2020; Zhang et al., 2023). Note that saltmarshes only survive at shoals with elevations above 2 m in the Yangtze Estuary. Among the four shoals, CM and NH (see profiles in Fig. 5) could provide such an elevation, likely forming the positive feedback loop between saltmarsh expansion, sediment trapping, and shoal accretion. The NH could limitedly favor saltmarsh growth after reclamation and most saltmarshes grow on the reclaimed area. The HS remains subtidal without vegetation occupation; hence, its erosion cannot be mitigated by saltmarshes. Although the saltmarsh expansion and the accretion on JD are strongly positively related, the invasive species *S. alterniflora* is more beneficial to accretion than the other species (Zhang et al., 2023). Specifically, the wave height reduction after 2009, when *S. alterniflora* was dominant, was further reduced by 0.4 m compared to that before 2006, when *S. mariqueter* was dominant (Zhang et al., 2023).

4.3. Implications for tidal flat management

The tidal flats in the mouth zone sustained accretion although the fluvial sediment supply has decreased since the mid-1980s. Previous studies have identified the morphological response time lag of 20–30 years in the HS and JD (Zhu et al., 2019) and this study has further indicated similar results for all the tidal flats in the mouth zone. Even though, the tidal flats in the mouth zone are eroded in recent years except for the JD. The accretion on the JD is closely related to the fast expansion of the dominant invasive species *S. alterniflora*; however, a policy on removing *S. alterniflora* in China has been implemented, aiming to effectively manage *S. alterniflora* by 2025, with a removal rate of over 90 % in each province. This strategy may have a profound effect on maintaining accretion on the JD and many other flats in the future. Note that the wetlands of CM and JD are national nature reserves and need to be urgently protected under global changes. Therefore, quantifying the sediment resources in both channels and shoals is essential to manage the tidal flats.

The sediment resources include two types: (1) mobile sediment, which can be sustainably reused; (2) fixed sediment, which is trapped in a certain area and usually is hardly reused. The mobile sediment mainly includes dredged materials in the channel and trapped sediment in the groin fields. The fixed sediment here includes the sediment in the reclaimed area and saltmarshes. Currently, there are no accurate estimates of the sediment sources deposited in the marshes and trapped by coastal engineering projects (i.e., dike structures to promote sediment accretion mainly for subsequent land reclamation) in the Yangtze Estuary, but we roughly estimated (Fig. 10). The estimation is based on the bathymetric maps, reclaimed and saltmarsh areas (see Fig. 4), and

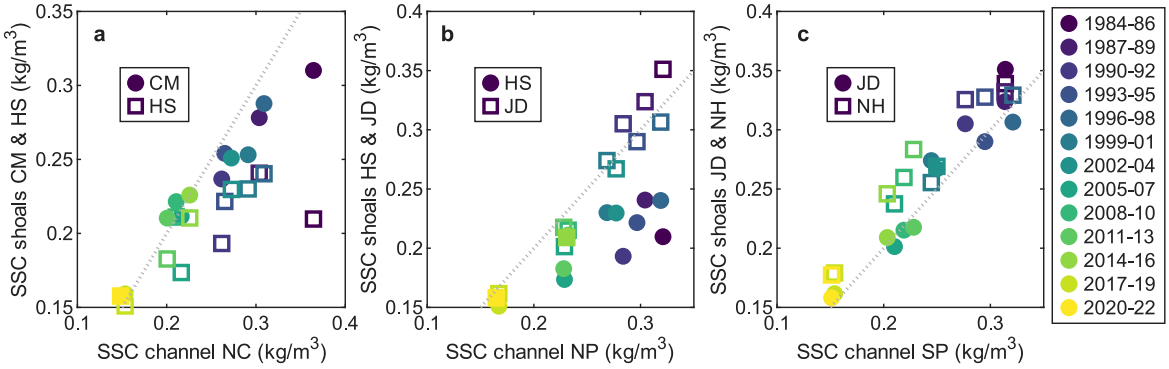

Fig. 9. The surface suspended sediment concentration (SSC) on shoals versus channels for the channel-shoal complexes **a** CM-NC-HS, **b** HS-NP-JD, **c** JD-SP-NH. The abbreviation of the channels and shoals refer to Fig. 1b. The filled cycles represent the northern shoals (**a** CM, **b** HS, **c** JD) whereas the hollow squares (**a** HS, **b** JD, **c** NH) represent the southern shoals in the complex. The dashed lines indicate the reference line where sediment concentrations are equal between channels and shoals. Data is obtained from Luo et al. (2022).

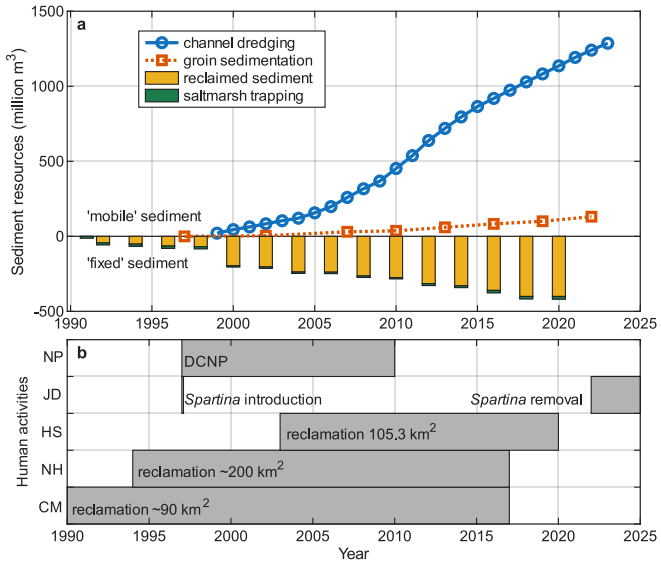

Fig. 10. **a** Cumulative change in sediment resources in terms of 'mobile' and 'fixed' sediment. **b** human activities in the North Passage (NP), Chongming flat (CM), Hengsha shoal (HS), Jiuduan shoal (JD), and Nanhui flat (NH). The Deep Channel Navigation Project (DCNP) was implemented in the NP (see Fig. 1b). The 'mobile' sediment includes the dredged sediments in the navigated NP, sedimentation above 0 m relative to 1997 in the groin field. The 'fixed' sediment includes the sediments in the reclaimed and saltmarsh areas.

assumptions on the elevation changes of reclaimed areas (assuming to make land for 1 m) and sedimentation rates of the saltmarshes and bare flats (assuming a sedimentation rate of 0.5 cm yr^{-1} (Wei et al., 2007),). The dredged material is a huge number of valuable resources with an annually dredged amount of 50 million m^3 yr^{-1}, which is nearly equivalent to the historical net deposition of channel-shoal complexes (see Fig. 8). The 50 million m^3 dredged materials could ideally result in sedimentation with a thickness of 12.5 cm on the HS. The beneficial use of dredged material has been one of the main strategies for sustainable management (called nature-based solutions) in estuaries worldwide (Baptist et al., 2019; Bose and Dhar, 2022; Carreira et al., 2025). Moreover, the sedimentation above 0 m in the groin field is generally trapped by groins because of the sheltering effects and part of the dredged material is also dumped to the groin field (Zhu et al., 2019). Therefore, the groin field becomes an important sediment storage with the amount of sediment reaching to 131 million m^3 in 2022 (an accretion rate of 5 million m^3 yr^{-1}). In contrast, the fixed sediment is much larger as the reclaimed sediment reaches 400 million m^3 in 2020 (rate of 13 million m^3 yr^{-1} during 1990–2020). The reclaimed sediment can no longer participate in morphodynamic feedback processes and therefore cannot serve as a sediment resource for promoting tidal flat development.

Generally, the growth of the tidal flat resources depends upon the quantity of sediment and the speed of the tidal flat being converted to land. Although the reclamation has been inhibited, global changes such as the fluvial sediment decline, storms, and sea-level rise still pose great threats to tidal flat evolution and therefore it is of high priority to make beneficial use of the mobile sediments. However, beneficial use of the mobile sediments needs to consider sediment properties, disposal locations, transport fates, assessment of the legal requirements, and many other practical issues, depending on the local settings (Baptist et al., 2019). Moreover, these sediments should be appropriately managed to minimize potential adverse consequences to the environment, ecology, and public health as they act as a sink of pollutants by accumulating metals (Zhang et al., 2019; Ferrans et al., 2021; Bose and Dhar, 2022). Further studies about how to beneficially use these materials need to be understood in the future.

5. Conclusions

This study has systematically analyzed the evolution of four large shoals in the Yangtze Estuary over a period of 64 years based on consistent bathymetric data. The results suggest that three of the four shoals, i.e., CM, HS, and NH, sustained accretion until 2010–2013 followed by a shift to erosion whereas JD keeps growing until nowadays, confirming the morphological response time lag of 20–30 years to reduced sediment supply.

The long-term shoal accretion is closely related to the sediment exchanges between channels and shoals, reclamation, and salt-marsh occupations. All the bifurcated channels have shown deepening and narrowing trends since 1997, which favors sediment trapping due to positive feedback effects between tidal deformation, sediment concentration, and hydraulic drag. The trapped sediments in the channel and offshore become important sediment sources to shoal accretion due to sediment exchange processes which contribute to a homogenous distribution of sediment concentration. These effects stand out as a prominent mechanism in sustaining shoal accretion in the first decades of sediment decline. Particularly surrounding the strongest deepened navigational channel, sediments have been nearly balanced in the central channel-shoal complex since 2010.

The land reclamation and saltmarshes enlarge the elevation differences between higher and lower shoals, resulting in steeper slopes of profiles and making shoals more vulnerable to forces like waves. Although reclamation has been regulated, the removal of invasive *S. alterniflora* which benefits accretion on JD (the only shoal that maintains accretion) would intervene in the accretion process, requiring further investigation. We propose that the abundant dredged sediments could be important sediment resources for sustainable tidal flat management.

CRediT authorship contribution statement

Chunyan Zhu: Writing – original draft, Visualization, Methodology, Funding acquisition, Conceptualization. **Weiming Xie:** Writing – review & editing, Investigation, Conceptualization. **Leicheng Guo:** Writing – review & editing, Funding acquisition. **Dirk Sebastiaan van Maren:** Writing – review & editing. **Wenting Wu:** Writing – review & editing, Methodology. **Fan Xu:** Writing – review & editing. **Yuan Xu:** Writing – review & editing. **Naiyu Zhang:** Writing – review & editing. **Zheng Bing Wang:** Writing – review & editing. **Qing He:** Writing – review & editing, Conceptualization.

Declaration of competing interest

The authors declare that they have no known competing financial interests or personal relationships that could have appeared to influence the work reported in this paper.

Acknowledgements

This work is financially supported by National Natural Science Foundation of China (NSFC, No. 42206169), National Key R&D Program of China (2023YFC3208500), and NSFC (Nos. U24A20181; 42576162; 42301540), China Postdoctoral Science Foundation (2022M721165, 2023T160219), Shanghai Pujiang Program (22PJD020). We acknowledge Wei Luo for sharing surface sediment concentration data derived from remote sensing as published in Luo et al. (2022).

Data availability

The bathymetric data that has been used is confidential.

References

Baptist, M.J., Gerkema, T., van Prooijen, B.C., van Maren, D.S., van Regteren, M., Schulz, K., Colosimo, I., Vroom, J., van Kessel, T., Grasmeijer, B., Willemsen, P., Elschot, K., de Groot, A.V., Cleveringa, J., van Eekelen, E.M.M., Schuurman, F., de Lange, H.J., van Puijenbroek, M.E.B., 2019. Beneficial use of dredged sediment to enhance salt marsh development by applying a 'Mud Motor.'. Ecol. Eng. 127, 312–323. https://doi.org/10.1016/j.ecoleng.2018.11.019.

Besset, M., Anthony, E.J., Bouchette, F., 2019. Multi-decadal variations in delta shorelines and their relationship to river sediment supply: an assessment and review. Earth Sci. Rev. 193, 199–219. https://doi.org/10.1016/j.earscirev.2019.04.018.

Bose, B.P., Dhar, M., 2022. Dredged sediments are one of the valuable resources: a review. IJESKA 4, 324–331.

Carreira, C., Bollwerk, S.M., Lønborg, C., 2025. A review on beneficial use of dredged marine sediment. Anthropocene Coasts 8, 12. https://doi.org/10.1007/s44218-025-00076-y.

Chen, J., Zhu, H., Dong, Y., Sun, J., 1985. Development of the changjiang estuary and its submerged delta. Continet. Shelf Res. Sediment Dynam. Changjiang Estuary Adjacent East China Sea 4, 47–56. https://doi.org/10.1016/0278-4343(85)90021-4.

Chen, Y., He, Q., Shen, J., Du, J., 2020. The alteration of lateral circulation under the influence of human activities in a multiple channel system, Changjiang Estuary. Estuarine. Coastal Shelf Sci. 242, 106823. https://doi.org/10.1016/j.ecss.2020.106823.

Colina Alonso, A., van Maren, D.S., Elias, E.P.L., Holthuijsen, S.J., Wang, Z.B., 2021. The contribution of sand and mud to infilling of tidal basins in response to a closure dam. Mar. Geol. 439, 106544. https://doi.org/10.1016/j.margeo.2021.106544.

de Jonge, V.N., Schuttelaars, H.M., van Beusekom, J.E.E., Talke, S.A., de Swart, H.E., 2014. The influence of channel deepening on estuarine turbidity levels and dynamics, as exemplified by the Ems estuary. Estuar. Coast Shelf Sci. 139, 46–59. https://doi.org/10.1016/j.ecss.2013.12.030.

de Vet, P.L.M., van Prooijen, B.C., Wang, Z.B., 2017. The differences in morphological development between the intertidal flats of the Eastern and Western Scheldt. Geomorphology 281, 31–42. https://doi.org/10.1016/j.geomorph.2016.12.031.

Dethier, E.N., Renshaw, C.E., Magilligan, F.J., 2022. Rapid changes to global river suspended sediment flux by humans. Science 376, 1447–1452. https://doi.org/10.1126/science.abn7980.

Edmonds, D.A., Toby, S.C., Siverd, C.G., Twilley, R., Bentley, S.J., Hagen, S., Xu, K., 2023. Land loss due to human-altered sediment budget in the Mississippi river Delta. Nat. Sustain. 6, 644–651. https://doi.org/10.1038/s41893-023-01081-0.

Elias, E.P.L., Van der Spek, A.J.F., Wang, Z.B., Cleveringa, J., Jeuken, C.J.L., Taal, M., Van der Werf, J.J., 2023. Large-scale morphological changes and sediment budget of the Western Scheldt estuary 1955–2020: the impact of large-scale sediment management. Neth. J. Geosci. 102, e12. https://doi.org/10.1017/njg.2023.11.

Fagherazzi, S., Priestas, A.M., 2010. Sediments and water fluxes in a muddy coastline: interplay between waves and tidal channel hydrodynamics. Earth Surf. Process. Landf. 35, 284–293. https://doi.org/10.1002/esp.1909.

Ferrans, L., Jani, Y., Burlakovs, J., Klavins, M., Hogland, W., 2021. Chemical speciation of metals from marine sediments: Assessment of potential pollution risk while dredging, a case study in southern Sweden. Chemosphere 263, 128105. https://doi.org/10.1016/j.chemosphere.2020.128105.

Gao, S., 2007. Modeling the growth limit of the Changjiang Delta. Geomorphology 85, 225–236. https://doi.org/10.1016/j.geomorph.2006.03.021.

Grandjean, T.J., Weenink, R., van der Wal, D., Addink, E.A., Hu, Z., Liu, S., Wang, Z.B., Yuan, L., Bouma, T.J., 2024. Critical turbidity thresholds for maintenance of estuarine tidal flats worldwide. Nat. Geosci. 17, 539–544. https://doi.org/10.1038/s41561-024-01431-3.

Guo, L., Zhu, C., Xie, W., Xu, F., Wu, H., Wan, Y., Wang, Z., Zhang, W., Shen, J., Wang, Z. B., He, Q., 2021. Changjiang Delta in the anthropocene: multi-scale hydro-morphodynamics and management challenges. Earth Sci. Rev. 223, 103850. https://doi.org/10.1016/j.earscirev.2021.103850.

Jalón-Rojas, I., Sottolichio, A., Hanquiez, V., Fort, A., Schmidt, S., 2018. To what extent multidecadal changes in morphology and fluvial discharge impact tide in a convergent (Turbid) tidal River. JGR Oceans 123, 3241–3258. https://doi.org/10.1002/2017JC013466.

Lenstra, K.J.H., Pluis, S.R.P.M., Ridderinkhof, W., Ruessink, G., van der Vegt, M., 2019. Cyclic channel-shoal dynamics at the Ameland inlet: the impact on waves, tides, and sediment transport. Ocean Dyn. 69, 409–425. https://doi.org/10.1007/s10236-019-01249-3.

Li, X., Liu, J.P., Tian, B., 2016. Evolution of the Jiuduansha wetland and the impact of navigation works in the Yangtze Estuary, China. Geomorphology 253, 328–339. https://doi.org/10.1016/j.geomorph.2015.10.031.

Lin, J., Prooijen, B.C. van, Guo, L., Zhu, C., He, Q., Wang, Z.B., 2021. Regime shifts in the Changjiang (Yangtze River) Estuary: the role of concentrated benthic suspensions. Mar. Geol. 433, 106403. https://doi.org/10.1016/j.margeo.2020.106403.

Lin, J., van Prooijen, B.C., Zhu, C., Guo, L., He, Q., Wang, Z.B., Yang, Q., 2025. Deepening and narrowing impacts on circulation, stratification, and sediment transport in the Changjiang Estuary. Front. Mar. Sci. 12. https://doi.org/10.3389/fmars.2025.1598417.

Luo, W., Shen, F., He, Q., Cao, F., Zhao, H., Li, M., 2022. Changes in suspended sediments in the Yangtze River Estuary from 1984 to 2020: responses to basin and estuarine engineering constructions. Sci. Total Environ. 805, 150381. https://doi.org/10.1016/j.scitotenv.2021.150381.

Mariotti, G., Fagherazzi, S., 2012. Channels-tidal flat sediment exchange: the channel spillover mechanism. J. Geophys. Res. 117. https://doi.org/10.1029/2011JC007378.

Murray, N.J., Phinn, S.R., DeWitt, M., Ferrari, R., Johnston, R., Lyons, Mitchell B., Clinton, Nicholas, Thau, David, Fuller, Richard A., 2019. The global distribution and trajectory of tidal flats. Nature 565, 222–225. https://doi.org/10.1038/s41586-018-0805-8.

Nienhuis, J.H., Kim, W., Milne, G.A., Quock, M., Slangen, A.B.A., Törnqvist, T.E., 2023. River deltas and sea-level rise. Annu. Rev. Earth Planet Sci. 51, 79–104. https://doi.org/10.1146/annurev-earth-031621-093732.

Ralston, D.K., Talke, S., Geyer, W.R., Al-Zubaidi, H.A.M., Sommerfield, C.K., 2019. Bigger tides, less flooding: effects of dredging on barotropic dynamics in a highly modified Estuary. JGR Oceans 124, 196–211. https://doi.org/10.1029/2018JC014313.

Syvitski, J., Ángel, J.R., Saito, Y., Overeem, I., Vörösmarty, C.J., Wang, H., Olago, D., 2022. Earth's sediment cycle during the anthropocene. Nat. Rev. Earth Environ. 3, 179–196. https://doi.org/10.1038/s43017-021-00253-w.

Talke, S.A., Jay, D.A., 2020. Changing tides: the role of natural and anthropogenic factors. Ann. Rev. Mar. Sci 12, 121–151. https://doi.org/10.1146/annurev-marine-010419-010727.

van Maren, D.S., Schrijvershof, R.A., Beemster, J., Zhu, C., Xie, D., Zhou, Z., Colina Alonso, A., Hoitink, A.J.F., 2025. Land reclamation impacts on tidal landscape evolution. Rev. Geophys. 63. https://doi.org/10.1029/2024RG000860.

van Maren, D.S., Winterwerp, J.C., Vroom, J., 2015. Fine sediment transport into the hyper-turbid lower Ems River: the role of channel deepening and sediment-induced drag reduction. Ocean Dyn. 65, 589–605. https://doi.org/10.1007/s10236-015-0821-2.

van Maren, D.S., Yang, S.-L., He, Q., 2013. The impact of silt trapping in large reservoirs on downstream morphology: the Yangtze River. Ocean Dyn. 63, 691–707. https://doi.org/10.1007/s10236-013-0622-4.

Wang, X., Xiao, X., Xu, X., Zou, Z., Chen, B., Qin, Yuanwei, Zhang, Xi, Dong, Jinwei, Liu, Diyou, Pan, Lianghao, Li, Bo, 2021. Rebound in China's coastal wetlands following conservation and restoration. Nat. Sustain. 4, 1076–1083. https://doi.org/10.1038/s41893-021-00793-5.

Wang, Z.B., Van Maren, D.S., Ding, P.X., Yang, S.L., Van Prooijen, B.C., De Vet, P.L.M., Winterwerp, J.C., De Vriend, H.J., Stive, M.J.F., He, Q., 2015. Human impacts on morphodynamic thresholds in estuarine systems. Cont. Shelf Res. 111, 174–183.

Wei, T., Chen, Z., Duan, L., Gu, J., Saito, Y., Zhang, W., Wang, Y., Kanai, Y., 2007. Sedimentation rates in relation to sedimentary processes of the Yangtze Estuary, China. Estuarine. Coastal Shelf Sci. Sedimentol. Ecohydrol. Processes Asian Deltas: Yangtze Mekong 71, 37–46. https://doi.org/10.1016/j.ecss.2006.08.014.

Wei, W., Dai, Z., Mei, X., Liu, J.P., Gao, S., Li, S., 2017. Shoal morphodynamics of the Changjiang (Yangtze) estuary: influences from river damming, estuarine hydraulic engineering and reclamation projects. Mar. Geol. 386, 32–43. https://doi.org/10.1016/j.margeo.2017.02.013.

Wei, W., Tang, Z., Dai, Z., Lin, Y., Ge, Z., Gao, J., 2015. Variations in tidal flats of the Changjiang (Yangtze) estuary during 1950s–2010s: future crisis and policy implication. Ocean Coast Manag. 108, 89–96. https://doi.org/10.1016/j.ocecoaman.2014.05.018.

Williams, R., 2012. DEMs of Difference. Geomorphological Techniques 2.

Winterwerp, J.C., Wang, Z.B., 2013. Man-induced regime shifts in small estuaries—I: theory. Ocean Dyn. 63, 1279–1292. https://doi.org/10.1007/s10236-013-0662-9.

Winterwerp, J.C., Wang, Z.B., van Braeckel, A., van Holland, G., Kösters, F., 2013. Man-induced regime shifts in small estuaries—Ii: a comparison of rivers. Ocean Dyn. 63, 1293–1306. https://doi.org/10.1007/s10236-013-0663-8.

Wu, W., Lin, Z., Chen, C., Chen, Z., Zhao, Z., Su, H., 2024a. Tracking the dynamics of tidal wetlands with time-series satellite images in the Yangtze River Estuary, China. Int. J. Digit. Earth 17, 2330684. https://doi.org/10.1080/17538947.2024.2330684.

Wu, W., Zhang, M., Chen, C., Chen, Z., Yang, H., Su, H., 2024b. Coastal reclamation shaped narrower and steeper tidal flats in Fujian, China: evidence from time-series satellite data. Ocean Coast Manag. 247, 106933. https://doi.org/10.1016/j.ocecoaman.2023.106933.

Xie, W., He, Q., Zhang, K., Guo, L., Wang, X., Shen, J., 2018. Impacts of human modifications and natural variations on short-term morphological changes in estuarine tidal flats. Estuaries Coasts 41, 1253–1267. https://doi.org/10.1007/s12237-017-0352-9.

Yang, H.F., Li, B.C., Yang, S.L., Zhang, Z.L., Xu, K.H., Chen, C.P., Ding, Y.F., Zhang, W.X., Shi, B.W., Wang, Y.P., 2022. Impacts of large projects on the sediment dynamics and evolution of the Hengsha Shoal in the Yangtze Delta. Ocean Eng. 261, 112030. https://doi.org/10.1016/j.oceaneng.2022.112030.

Yang, S.L., Luo, X., Temmerman, S., Kirwan, M., Bouma, T., Xu, K., Zhang, S., Fan, J., Shi, B., Yang, H., Wang, Y.P., Shi, X., Gao, S., 2020. Role of delta-front erosion in sustaining salt marshes under sea-level rise and fluvial sediment decline. Limnol. Oceanogr. 65, 1990–2009. https://doi.org/10.1002/lno.11432.

Yang, S.L., Milliman, J.D., Li, P., Xu, K., 2011. 50,000 dams later: erosion of the Yangtze River and its delta. Global Planet. Change 75, 14–20. https://doi.org/10.1016/j.gloplacha.2010.09.006.

Zhang, M., Dai, Z., Bouma, T.J., Bricker, J., Townend, I., Wen, J., Zhao, T., Cai, H., 2021. Tidal-flat reclamation aggravates potential risk from storm impacts. Coast. Eng. 166, 103868. https://doi.org/10.1016/j.coastaleng.2021.103868.

Zhang, M., Schwarz, C., Lin, W., Naing, H., Cai, H., Zhu, Z., 2023. A new perspective on the impacts of Spartina alterniflora invasion on Chinese wetlands in the context of climate change: a case study of the Jiuduansha shoals, Yangtze Estuary. Sci. Total Environ. 868, 161477. https://doi.org/10.1016/j.scitotenv.2023.161477.

Zhang, H., Walker, T.R., Davis, E., Ma, G., 2019. Ecological risk assessment of metals in small craft harbour sediments in Nova Scotia, Canada. Marine Pollution Bulletin 146, 466–475. https://doi.org/10.1016/j.marpolbul.2019.06.068.

Zhang, X., Xie, R., Fan, D., Yang, Z., Wang, H., Wu, C., Yao, Y., 2021. Sustained growth of the largest uninhabited alluvial island in the Changjiang Estuary under the drastic

reduction of river discharged sediment. Sci. China Earth Sci. 64, 1687–1697. https://doi.org/10.1007/s11430-020-9746-3.

Zhou, S., Zhu, C., Lin, J., Xie, W., Zhang, N., Guo, L., He, Q., 2025. Multi-asymmetry on residual sediment transport in the branching channels of the Yangtze Estuary. J. Hydrol., 132947 https://doi.org/10.1016/j.jhydrol.2025.132947.

Zhou, Z., Ge, J., van Maren, D.S., Wang, Z.B., Kuai, Y., Ding, P., 2021. Study of sediment transport in a tidal channel-shoal system: lateral effects and slack-water dynamics. J. Geophys. Res.: Oceans 126. https://doi.org/10.1029/2020JC016334 e2020JC016334.

Zhu, C., Guo, L., van Maren, D.S., Tian, B., Wang, X., He, Q., Wang, Z.B., 2019. Decadal morphological evolution of the mouth zone of the Yangtze Estuary in response to human interventions. Earth Surf. Process. Landf. 44, 2319–2332. https://doi.org/10.1002/esp.4647.

Zhu, C., van Maren, D.S., Guo, L., Lin, J., He, Q., Wang, Z.B., 2022. Feedback effects of sediment suspensions on transport mechanisms in an estuarine turbidity maximum. JGR Oceans 127. https://doi.org/10.1029/2021JC018029 e2021JC018029.

Zhu, C., van Maren, D.S., Guo, L., Lin, J., He, Q., Wang, Z.B., 2021. Effects of sediment-induced density gradients on the estuarine turbidity maximum in the Yangtze Estuary. JGR Oceans 126. https://doi.org/10.1029/2020JC016927 e2020JC016927.

Zhu, C., van Maren, D.S., Guo, L., Xie, W., Xing, C., Wang, Z.B., He, Q., 2025. Water and sediment exchange between the anthropogenically modified distributaries of the Yangtze Estuary. Catena 250, 108729. https://doi.org/10.1016/j.catena.2025.108729.

Zhu, L., He, Q., Shen, J., 2018. Modeling lateral circulation and its influence on the along-channel flow in a branched estuary. Ocean Dyn. 68, 177–191. https://doi.org/10.1007/s10236-017-1114-8.

Zhu, Q., Xing, F., Wang, Y.P., Syvitski, J., Overeem, I., Guo, J., Li, Y., Tang, J., Yu, Q., Gao, J., Gao, S., 2024. Hidden delta degradation due to fluvial sediment decline and intensified marine storms. Sci. Adv. 10. https://doi.org/10.1126/sciadv.adk1698 eadk1698.